Available online at www.sciencedirect.com
ScienceDirect
Surface & Coatings Technology 202 (2008) 3519–3528
SURFACE & COATINGS TECHNOLOGY
www.elsevier.com/locate/surfcoat

Influence of normal load and sliding speed on the tribological property of amorphous carbon nitride coatings sliding against Si_3N_4 balls in water

Fei Zhou [a,*], Xiaolei Wang [b], Koshi Adachi [c], Koji Kato [c]

[a] Academy of Frontier Science, Nanjing University of Aeronautics and Astronautics, Nanjing, 210016, PRChina
[b] School of Mechanical Engineering, Nanjing University of Aeronautics and Astronautics, 210016, PRChina
[c] Laboratory of Tribology, School of Mechanical Engineering, Tohoku University, Sendai, 980-8579, Japan

Received 20 October 2007; accepted in revised form 18 December 2007
Available online 31 January 2008

Abstract

Amorphous carbon nitride (a–CN_x) coatings were deposited on Si_3N_4 disks by an ion beam assisted deposition system. The composition, structure and hardness of the a–CN_x coatings were characterized by Auger electronic spectroscopy, Raman spectroscopy and nano-indentation tester, respectively. The influences of normal load and sliding speed on the friction coefficients and the specific wear rates for the a–CN_x/Si_3N_4 tribo-pairs were investigated and analyzed synthetically by ball-on-disk tribometer. The worn surfaces were observed by optical microscope. The results showed that the a–CN_x coatings contained 12 at.% nitrogen, and their structure was a mixture of $sp^2$and sp^3 bonds. The a–CN_x coatings' nanohardness was 29 GPa. The influence of sliding speed on the friction coefficients and the specific wear rate of the CN_x coatings was more obvious than that of normal load. The friction coefficients and the specific wear rate of the CN_x coatings decreased as the sliding speed increased. At a sliding speed higher than 0.1 m/s, the friction coefficients were less than 0.04. The specific wear rates of the a–CN_x coatings were higher than those of Si_3N_4 balls at a sliding speed below 0.1 m/s, while the specific wear rates of the a–CN_x coatings and the Si_3N_4 balls all fluctuated around a lower level of 10^{-8} mm^3/Nm as the sliding speed increased beyond 0.2 m/s. To describe the wear behavior of a–CN_x coatings sliding against Si_3N_4 balls in water with normal loads of 3–15 N and sliding speeds of 0.05–0.5 m/s, the wear-mechanism map for the a–CN_x/Si_3N_4 tribo-pairs in water was developed.

Keywords: Amorphous CN_x coatings; Si_3N_4 balls; Friction; Wear; Water lubrication; Wear-mechanism map

1. Introduction

Water lubrication systems are expected to replace conventional oil lubrication systems to protect natural environment [1]. However, water lubrication systems present some technical problems for metallic materials, such as lubricity, corrosion and reliability. The recent technical approach to water lubrication systems is to use engineering ceramics or plastics [2]. Due to insufficient strength and microstructure ageing, engineering plastics could not be applied to water lubrication system for longer period of time [3]. It is well known that the self-mated SiC (Si_3N_4) ceramics exhibit good lubricity in water environments [4–15]. Due to the longer running-in period for SiC/SiC tribo-pairs in water and the easy occurrence of hydration reaction between SiC(Si_3N_4) and water, severe wear was easily observed for the self-mated SiC(Si_3N_4) tribopair in water [8,10,13]. Currently, two methods are used to enhance anti-wear ability of SiC(Si_3N_4) ceramics in water: (1) the addition of second phase [9,12–14]; (2) surface coating [15–21]. It is evident that TiC or TiC–TiB_2 particles could enhance the anti-wearability of SiC ceramics in water, but worsen the friction behavior of SiC ceramics in water lubrication [9]. If short carbon fibers were added Si_3N_4 ceramics, lower friction coefficients and specific wear rates of composites were obtained simultaneously than those of the self-mated Si_3N_4 tribopairs [12,13]. Saito T. et al reported that h–BN could shorten the running-in period of the self-mated Si_3N_4 tribopairs and improve their friction property, but could not enhance their wear resistance [14]. As highly disordered or amorphous carbon /graphite layers were deposited on SiC ceramic, low friction and low wear were obtained

* Corresponding author. Tel./fax: +86 25 84892581 803.
E-mail addresses: fzhou@nuaa.edu.cn, zhoufei88cn@yahoo.com.cn (F. Zhou).

0257-8972/$ - see front matter © 2007 Elsevier B.V. All rights reserved.
doi:10.1016/j.surfcoat.2007.12.025

successfully [16,17]. If the a–CN_x coatings were deposited on SiC disk, the wear resistance of SiC ball in water was greater than that of SiC/SiC tribo-pair in water [15]. When the *a–CN_x* coatings slid against SiC or Si_3N_4 balls at 5 N and 0.16 m/s in water, the lower friction coefficient of 0.01–0.02 was achieved [18], and then the wear-mechanism map of the a–CN_x/SiC tribo-pair in water was established [19]. Under the same frictional conditions, the friction and wear properties of the a–CN_x/SiC tribo-couple in water are superior to those of the a–C/SiC tribo-pair [20]. Recently, the a–CN_x coatings have reportedly improved the friction and wear properties of Si_3N_4 ceramics in water [21]. However, the influences of sliding velocity (V) and normal load (W) on the friction and wear property of the a–CN_x/Si_3N_4 tribo-couple in water have not yet been studied synthetically. Therefore, the present purpose is to investigate the variation of friction coefficients and specific wear rates of tribo-materials in the a–CN_x/Si_3N_4 tribo-couple with normal load and sliding velocity, and to develop the wear-mechanism map of the a–CN_x/Si_3N_4 tribo-couples in water.

2. Experimental procedures

2.1. Coating method

The ion beam assisted deposition (IBAD) machine (Hitachi Ltd, Japan) was used to deposit the a–CN_x coatings [15]. Prior to IBAD process, Si_3N_4 disks (Ø30 mm × 4 mm) were ultrasonically cleaned in acetone and ethanol for 30 min. Then, a substrate jig containing a Si_3N_4 disk was mounted on the substrate holder with two screws and a carbon target with purity of 99.99% was also put into an electron beam evaporator. After that, the deposition chamber doors were closed and the vacuum chamber was subsequently evacuated. When the vacuum chamber pressure was lower than 2.0×10^{-4} Pa, the deposited surface was bombarded with nitrogen ions for 5 min. The accelerated voltage and current density for nitrogen ions were 1.0 kV and 100 μA/cm^2, respectively. Later, the a–CN_x coatings were synthesized by mixing carbon vapor and energetic N ions. Energetic N ions were produced at 1.5 kV and 90 μA/cm^2. Carbon vapor was formed by heating a graphite target with an electron beam evaporator. The evaporation rate was 2 nm/s, which was controlled by adjusting the carbon vapor emission current. The coating's thickness was 0.5 μm.

2.2. Composition and microstructure analysis of a–CN_x coatings

The surface atomic composition and microstructure of the a–CN_x coatings were analyzed by Auger electron spectroscopy (AES) and Raman spectroscopy (Dilor-Jobin yvon-Spex, Labram), respectively.

2.3. Surface roughness and mechanical properties of tribo-materials

The surface roughness of tribo-materials such as Si_3N_4 balls (Ø8 mm), Si_3N_4 disks and the a–CN_x coatings was measured by Surfcom-1500DX profilometer (Tokyo, Japan). To obtain the surface roughness accurately, at least 5 measurement tests were carried out for each specimen.

The mechanical properties of Si_3N_4 balls and Si_3N_4 disks were acquired from the balls' manufacturer, whereas the mechanical properties of the a–CN_x coatings were evaluated using ENT-1100A nano-indentation hardness tester (Elionix Co. Ltd., Japan) with a Berkovich-typed diamond indenter. The maximum load was 980 μN. The time for loading and unloading was set at 10 s. The indentation penetration depth obtained for the a–CN_x coatings ranged from 50 to 60 nm.

2.4. Ball-on-disk wear test

Prior to each wear test, all samples were cleaned in acetone and ethanol ultrasonically for 30 min. The experiments were performed on a ball-on-disk apparatus which consisted of rotating disk sliding against a stationary ball at the sliding speed in the range of 0.05~0.5 m/s with a normal load of 3 to15 N. The rubbing surfaces were submerged in distilled water at room temperature. The total sliding distance was 3000 m. The friction forces were detected by a LMA-A-10 N load cell (Kyowa Co. LTD, Japan). The load cell voltage was measured by a DPM-700B strain amplifier (Kyowa Co. LTD, Japan) and recorded by NR-110/150 data collection system (Keyence Co. LTD, Japan) with a compatible personal computer. The diameter of Si_3N_4 ball's wear scar under each condition was measured using a Keyence VH-8000 optical microscope (Keyence Co. LTD, Japan). The cross-section area, A, of wear track on the disk was determined using a Tencor P-10 surface profilometer (Kurashiki Kako Co. LTD, Japan). Thus, the specific wear rates for balls and coatings were calculated using the following equation:

$$w_{s,b} = \frac{3.14d^4}{64\mathrm{RWL}} \tag{1}$$

$$w_{s,d} = \frac{2\pi rA}{\mathrm{WL}} \tag{2}$$

where R is the ball radius, d is the diameter of the ball wear scar, r is the disk wear track radius, W is normal load and L is total sliding distance. Moreover, the wear track on the disk and the

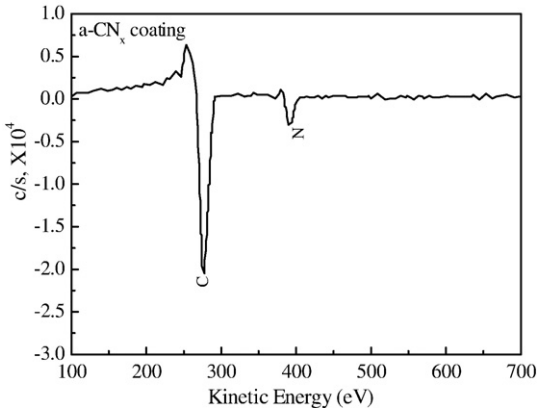

Fig. 1. Auger electron spectra of a–CN_x coatings.

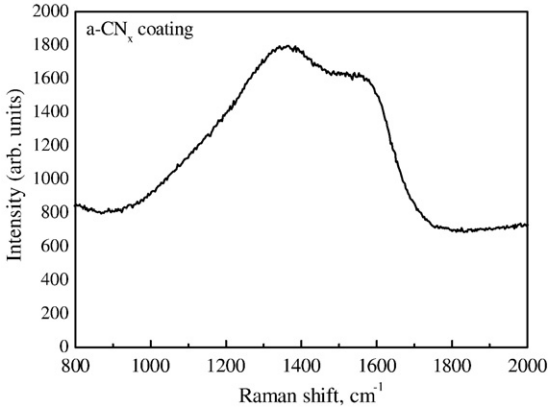

Fig. 2. Raman spectra of a–CN_x coatings.

ball wear scar were observed using Keyence VH-8000 optical microscope.

3. Results and discussion

3.1. Composition and microstructure of a–CN_x coatings

According to the AES analysis shown in Fig. 1, the a–CN_x coatings contained 12 at.% nitrogen. In comparison to the a–C coatings [22], the Auger electron energy of carbon hybrided with nitrogen in the a–CN_x coating decreased. The results in Fig. 2 show that the Raman spectrum of the a–CN_x coatings had a broad and skew peak ranging from 1200 to 1700 cm^{-1}, which was composed of the overlapping D-peak (centered round 1300–1450 cm^{-1}) and the G-peak (centered round 1550–1580 cm^{-1}). The G-peak corresponded to graphite-like layers of sp^2 micro-domains in the coating, while the D-peak was attributed to bond angle disorder in the graphite-like micro-domains induced by linking with sp^3 carbon atoms as well as the finite crystalline sizes of sp^2 micro-domains in the coatings [23]. Thus, it is concluded that the a–CN_x coatings' structure was a mixture of $sp^2$and sp^3 bond. As seen in Table 1, in comparison to the a–C coatings, the G-peak of the a–CN_x coatings shifted to higher frequencies while the D-peak of the a–CN_x coatings shifted to lower frequencies. Furthermore, the intensity ratio of D-band to G-band (I_D/I_G) for the a–CNx coatings increased (Table 1). Zhang S. et al [24] reported that the sp^3 fraction in the a–C coatings was inversely proportional to the intensity ratio (I_D/I_G). This indicates that the a–CN_x coatings' sp^2 fraction increased.

3.2. Surface roughness and mechanical properties of a–CN_x coatings

As seen in Table 2, the arithmetic mean roughness R_a of the a–CN_x coating was a little lower than that of the Si_3N_4 substrate.

Table 1
D- and G- peak frequencies and their intensity ratio

Coating	ω_D, cm^{-1}	ω_G, cm^{-1}	I_D/I_G
a-C [22]	1375	1560	1.07
a–CN_x	1350	1575	1.11

Table 2
Surface roughness and mechanical properties of Si_3N_4 ball, a–CN_x coatings and Si_3N_4 disk

Name	R_a,μm	H, GPa	E, GPa
Si_3N_4 ball	0.0552	15.3 [a]	308 [a]
a–CN_x	0.0251	29±2	330±20
Si_3N_4 disk	0.0280	16 [a]	290 [a]

[a] The data are from the sample manufacturer.

This indicated that the energetic particle bombardment enhanced the mobility of carbon atoms on the growing surface and induced the smooth surface. Fig. 3 displays nano-indentation load vs. indentation depth curve for the a–CN_x coatings. According to the standard Oliver and Pharr approach [25], the mean values of elastic modulus (E) and hardness (H) for the a–CN_x film were calculated from the nano-indentation load-displacement curve (Fig. 3) and listed in Table 2. It is clear that the a–CN_x coatings offered a combination of reasonably high hardness and reduced stiffness while achieving remarkable elastic recovery. This indicates that the a–CN_x coatings' sp^2 fraction increased in order to improve the tribological property of the a–CN_x films (low friction coefficient and better durability).

3.3. Dependence of the friction coefficient and wear rate on the normal load

Fig. 4 shows the variation of friction coefficients with sliding distance at various normal loads for the a–CN_x/Si_3N_4 tribopairs in water. It is evident that the running-in distance (the sliding distance as the steady-state friction coefficient is obtained) became short as the normal load increased. The phenomena were identical to Ref.[15]. At 0.05 m/s, with an increase in sliding distance, the friction coefficient first decreased gradually, then reached the stable values at 3, 6, 9 and 15 N, but at 12 N, the friction coefficient suddenly increased to 0.09, and then fluctuated around 0.093 (Fig. 4(a)). If the sliding speed was larger than 0.02 m/s, the friction coefficient decreased initially to the steady-state value, and the stable friction coefficient differences among five kinds of the normal loads became small (Fig. 4 (b)~(d)) at increasing sliding speed. At 0.5 m/s, the stable

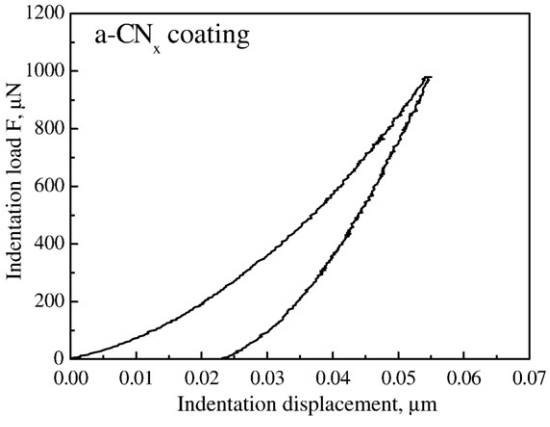

Fig. 3. Nano-indentation load vs. indentation displacement curve for a–CN_x coatings.

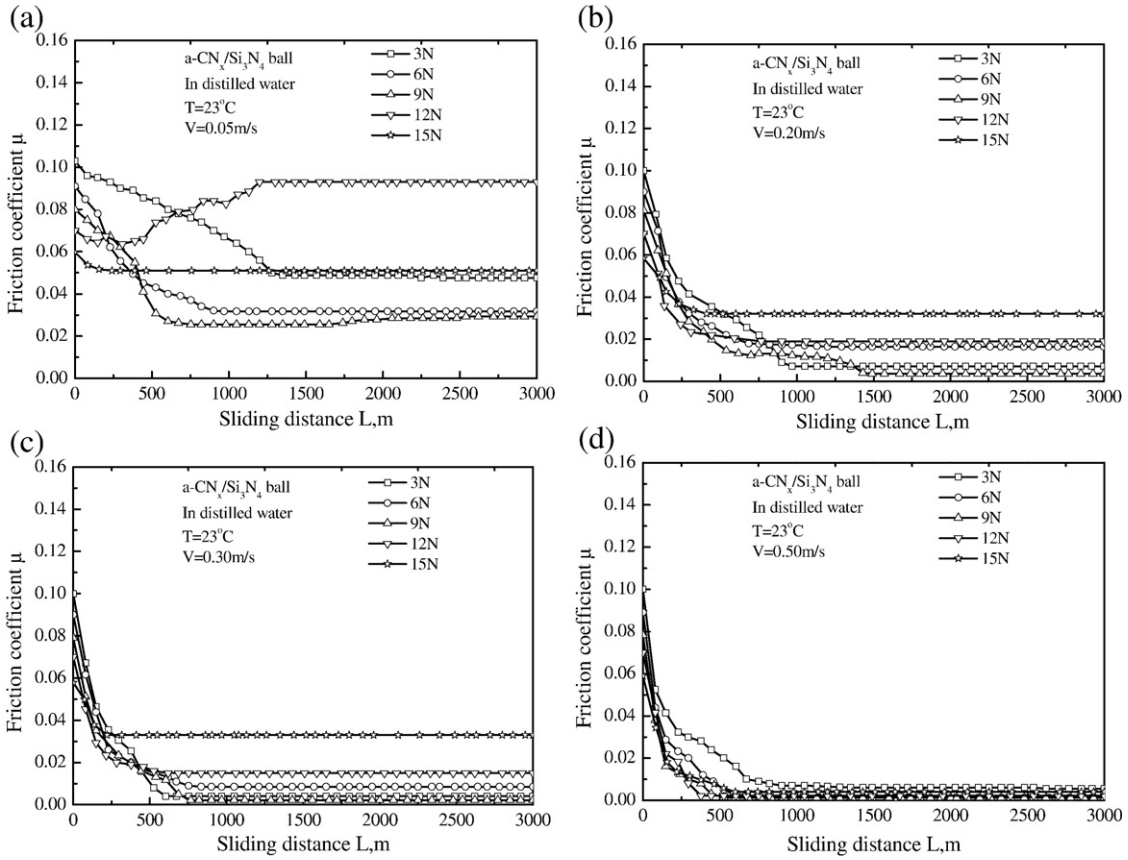

Fig. 4. Variation of friction coefficient with sliding distance at various sliding speeds in water.

friction coefficient varied in the range of 0.001~0.006. Fig. 5 displays the variation of mean steady-state friction coefficient (μ_m) with normal load (W) for the a–CN_x/Si_3N_4 tribo-pair in water. At 0.05 m/s, the mean stable friction coefficients varied in the range of 0.027~0.051. But at 12 N, the value of μ_m was 0.093. If the sliding speed was 0.5 m/s, the mean steady-state friction coefficient fluctuated slightly in the range of 0.001~0.006. When the sliding speed fluctuated in the range of 0.1~0.3 m/s, the variation curves of μ_m vs. W zigzagged.

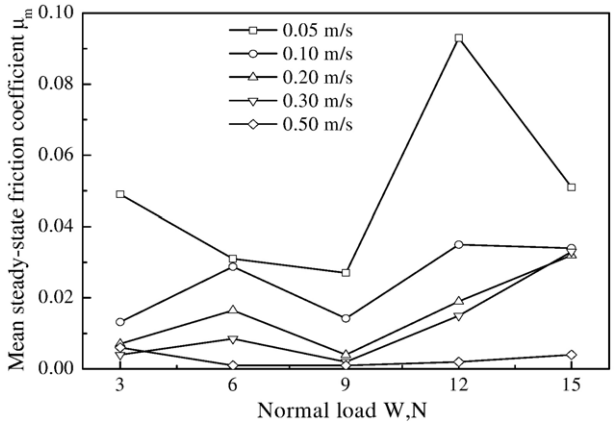

Fig. 5. Influence of normal load on mean steady-state friction coefficient for the a–CN_x/Si_3N_4 tribo-pair in water.

As seen in Fig. 6(a), the influence of normal loads on the specific wear rate of Si_3N_4 ball was not obvious. With an increase in the normal load, the specific wear rate of Si_3N_4 ball always fluctuated in the range of 0.6×10^{-8}~3.6×10^{-8} mm^3/Nm. But at 15 N and 0.05 m/s, the specific wear rate of Si_3N_4 ball reached peak of 9.0×10^{-8} mm^3/Nm. Fig. 6(b) shows that the normal loads markedly influenced the a–CN_x coatings' specific wear rate at a sliding speed lower than 0.1 m/s. At 0.05 m/s, the curve of w_{sc} *vs.* W for the a–CN_x coatings zigzagged. With an increase in the normal load, the a–CN_x coatings' specific wear rate varied in the range of 10.5×10^{-8}~20.4×10^{-8} mm^3/Nm. If the sliding speed reached 0.1 m/s, the specific wear rates of the a–CN_x coatings first increased, and then decreased gradually with increasing normal load. As the sliding speed varied in the range of 0.2~0.5 m/s, the a–CN_x coatings' specific wear rate fluctuated slightly in the range of 2.5×10^{-8}~6.5×10^{-8} mm^3/Nm with an increase in the normal load. It is evident from Fig. 6 that the normal load had no obvious influence on the Si_3N_4 balls' specific wear rate, but had marked influence on the a–CN_x coatings' specific wear rates at a sliding speed below 0.1 m/s. When the sliding speed was higher than 0.1 m/s, the normal load displayed the slight influence on the a–CN_x coatings' specific wear rates. Furthermore, the specific wear rate of the a–CN_x coatings were higher than those of Si_3N_4 balls at a sliding velocity under 0.1 m/s, whereas their specific wear rates all fluctuated around the lowest level of 10^{-8} mm^3/Nm at sliding velocities above 0.2 m/s.

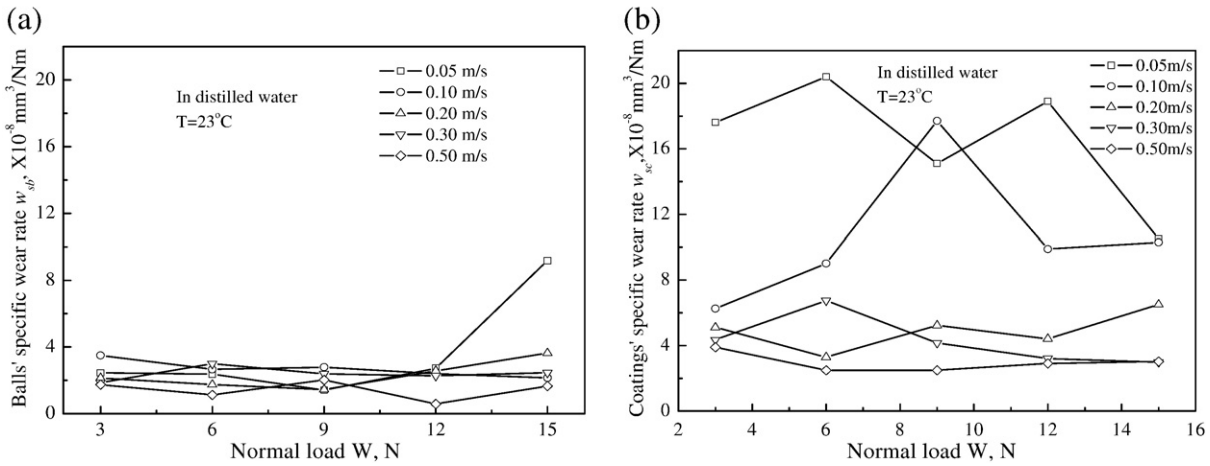

Fig. 6. Influence of normal load on specific wear rates of Si_3N_4balls (a)and the a–CN_x coatings (b).

3.4. Dependence of the friction coefficient and wear rate on the sliding speed

Fig. 7 shows the variation of friction coefficients with sliding distance at various sliding speeds for the a–CN_x/Si_3N_4 tribopairs in water. The initial friction coefficient decreased as the normal load increased, and the friction coefficient at 0.05 m/s was highest in every figure. With an increase in the sliding distance, the friction coefficient decreased during running-in distance and then varied around the stable values. At 3 N, the running-in period decreased as the sliding speed increased. At a sliding speed lower than 0.1 m/s, the stable friction coefficient was above 0.01. As the sliding speed varied in the rage of 0.2~0.5 m/s, the stable friction coefficient fluctuated in the range of 0.004~0.007 as sliding distance increased (Fig. 7(a)). If the normal load was 6 N, the friction coefficient decreased as the sliding speed increased. At a sliding speed lower than 0.1 m/s, the friction coefficient first decreased from 0.09 to 0.03, and then varied in the range of 0.028~0.031 as the sliding distance increased. If the sliding speed was higher than 0.1 m/s, as the

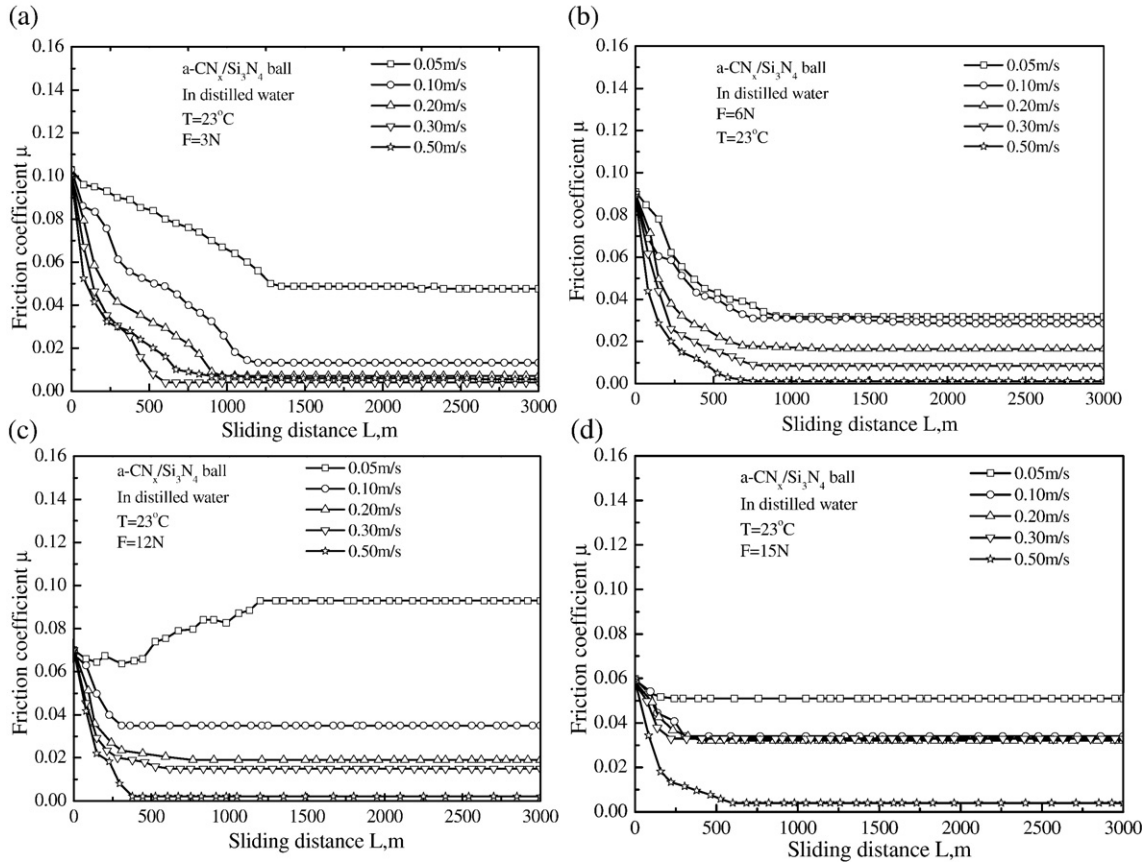

Fig. 7. Variation of friction coefficient with sliding distance at various normal loads in water.

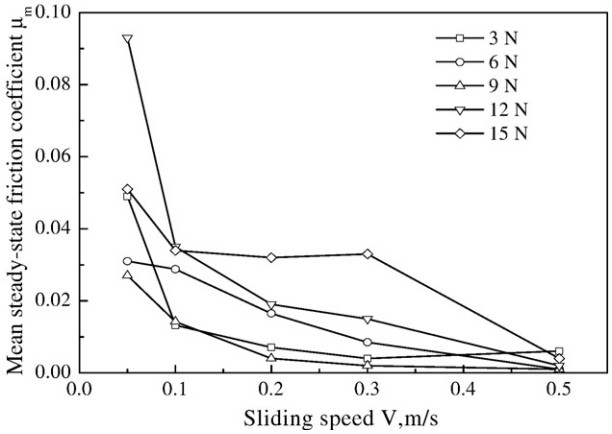

Fig. 8. Influence of sliding speed on mean steady-state friction coefficient for the a–CN_x/Si_3N_4 tribo-pair in water.

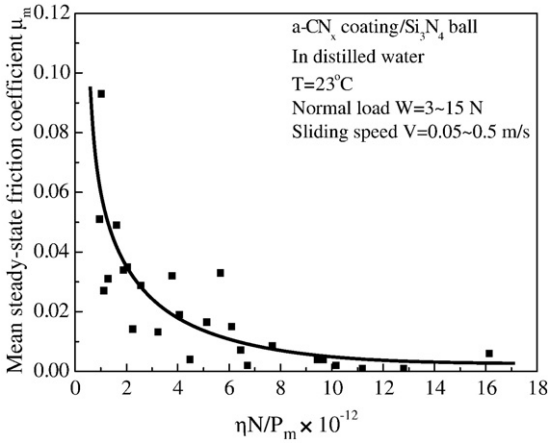

Fig. 10. Stribeck curves of the a–CN_x/Si_3N_4 tribo-pair in water after running-in.

sliding distance increased, the friction coefficient initially decreased from 0.09 to different stable value, such as 0.016 at 0.2 m/s, 0.008 at 0.3 m/s and 0.001 at 0.5 m/s (Fig. 7(b)). Fig. 7(c) shows that the friction coefficient at 0.05 m/s first varied in the range of 0.065~0.07 at a sliding distance shorter than 440 m, and then increased gradually from 0.065 to 0.093 when the sliding distance varied in the range of 440~1200 m. Finally, it approached 0.093. If the sliding speed was higher than 0.05 m/s, the friction coefficient initially decreased from 0.07 to the different stable values as the sliding distance increased. At 15 N, when the sliding speed ranged from 0.1 to 0.3 m/s, the friction coefficient first decreased from 0.06 to 0.033 at a sliding distance shorter than 320 m, then fluctuated in the range of 0.032~0.034 with further sliding. But at 0.05 or 0.5 m/s, the friction coefficients first decreased from 0.06 to 0.051 or 0.004, and then fluctuated slightly around stable values as the sliding distance increased (Fig. 7(d)). Fig. 8 shows the variation of mean steady-state friction coefficient (μ_m) with sliding speed (V) for the a–CN_x/Si_3N_4 tribo-pair in water. It is clear that the friction coefficient decreased gradually as the sliding velocity increased. The mean steady-state friction coefficients were lower than 0.04 when the sliding speed was higher than 0.1 m/s.

Fig. 9 displays the influence of sliding speed on the specific wear rates of Si_3N_4 balls and the a–CN_x coatings. With an increase in sliding velocity, the specific wear rates of Si_3N_4 balls fluctuated in the range of 0.6×10^{-8}~3.6×10^{-8} mm^3/Nm. But at 15 N and 0.05 m/s, the specific wear rate of Si_3N_4 ball was 9.0×10^{-8} mm^3/Nm (Fig. 9a). As seen in Fig. 9(b), it is clear that a downward trend of the a–CN_x coatings' specific wear rates with sliding speed was observed. The results in Fig. 9 indicate that the sliding speed had no marked influence on the specific wear rate of the Si_3N_4 balls, but had negative influence on the specific wear rates of the a–CN_x coatings. At a sliding velocity higher than 0.2 m/s, the specific wear rates of the a–CN_x coatings and Si_3N_4 balls all fluctuated around the lowest level of 10^{-8} mm^3/Nm.

3.5. Water-lubrication mechanism of the a–CN_x/Si_3N_4 tribopair

To elucidate the water lubrication mechanism of the a–CN_x/Si_3N_4 tribo-pair, the data in Fig. 5 were rearranged and a type of

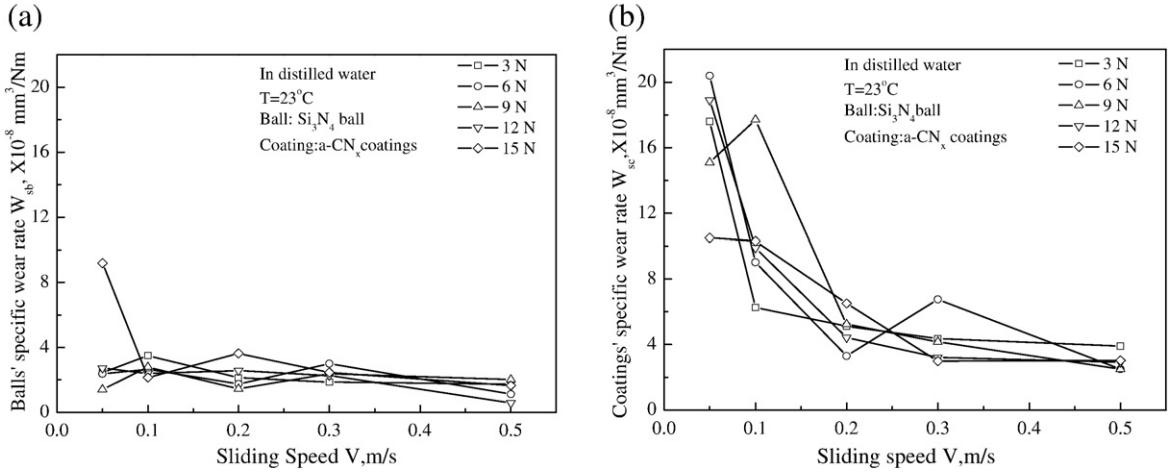

Fig. 9. Influence of sliding speed on specific wear rates of Si_3N_4balls (a)and the a–CN_x coatings (b).

Table 3
Friction and wear properties of the a–CN_x/Si_3N_4 in water in four regions

Region	I	II	III	IV
Friction coefficient μ	$0.032<\mu<0.093$	$0.014<\mu<0.049$	$0.004<\mu<0.029$	$0.001<\mu<0.008$
Coatings' wear rate w_{sc}, $\times 10^{-8}$ mm^3/Nm	$6.5<w_{sc}<18.9$	$3.0<w_{sc}<20.4$	$3.2<w_{sc}<9.0$	$2.5<w_{sc}<6.8$
Wear rate of Si_3N_4 ball w_{sb}, $\times 10^{-8}$ mm^3/Nm	$2.2<w_{sb}<9.2$	$1.4<w_{sb}<2.8$	$1.4<w_{sb}<3.5$	$0.6<w_{sb}<3.0$
Observation of worn surface	a–CN_x coatings delamination and severe scratches	Smooth surface with deeper scratches	Smooth surface with deep scratches	Smooth surface
Wear-mechanism	MW	MW+PTW	PMW+TW	TW

stribeck curve is illustrated in Fig. 10. The relationship between μ_m and the Sommerfeld number $\eta N/P$ (P is mean contact pressure, N is rotating velocity, η is the dynamic viscosity of lubricant) indicated that there was a critical Sommerfeld number for the a–CN_x/Si_3N_4 tribo-couple. When a Sommerfeld number was smaller than the critical value, the friction coefficient increased abruptly to 0.093 with decreasing Sommerfeld number. When the Sommerfeld number was higher than the critical value, the friction coefficient decreased gradually with an increase in Sommerfeld number. This indicated that the lubrication mechanism changed from mixed lubrication (ML) to boundary lubrication (BL) as the Sommerfeld number decreased Xu J. et al [8] reported that the water lubrication of silicon nitride involved both hydrodynamic lubrication (HL) by water and BL by the hydrated silica layers. But for the a–CN_x/Si_3N_4 tribo-couple, at 15 N or 0.05 m/s, the water lubrication film broke down easily and solid-to-solid contact was established, so the friction coefficient increased abruptly and the lubrication mechanism was BL. With an increase in sliding speed or a decrease in normal load, the applied load was supported by both a HL film (water film) and a BL film (tribolayer), thus, the lubrication mechanism became ML.

3.6. Wear-mechanism map

After the experimental data and the worn surfaces were classified and tabulated in Table 3, the wear-mechanism map of the a–CN_x/Si_3N_4 ball in water was illustrated in Fig. 11. The normal load (W)-Sliding velocity (V) diagram was divided into four regions. As seen in Fig. 11, when the experimental parameters were located in the first area (I), the friction coefficient of the a–CN_x/Si_3N_4 tribo-couple varied in the range of 0.032~0.093, and the specific wear rates of the a–CN_x coating and Si_3N_4 ball fluctuated in the range of 6.5×10^{-8}~18.9×10^{-8} and 2.2×10^{-8}~9.2×10^{-8} mm^3/Nm, respectively. The worn surfaces on Si_3N_4 ball and the a–CN_x coatings were covered with many deepest scratch lines parallel to the sliding direction. Furthermore, the a–CN_x coatings were partially delaminated (Fig. 12). In the first area (I), the normal load was highest and the sliding speed was lowest. The water lubrication film easily broke down and solid-to-solid contact was established, so the friction coefficient increased under boundary lubrication. Refs.[1,8,10] reported that the mechanical wear was characterized mainly by the formation of microcracks in the subsurface and the occurrence of microfracture. This indicated that the lubrication mechanism was BL and the wear mechanism in the first region (I) was mechanical wear (MW). As the experimental parameters were located in the second area (II) the friction coefficient of the a–CN_x/Si_3N_4 tribo-couple ranged from 0.014 to 0.049, and the specific wear rates of the a–CN_x coating and Si_3N_4 ball fluctuated in the range of 3.0×10^{-8}~20.4×10^{-8} and 1.4×10^{-8}~2.8×10^{-8} mm^3/Nm, respectively. The worn surface on Si_3N_4 ball and the a–CN_x coatings were smooth and flat aside from some deeper scratches (Fig. 13). Refs. [1,8,10] indicated that the tribochemical wear was characterized by a smooth and flat surface and the delamination and dissolution of hydration reaction products. This indicated that the partial tribochemical reactions between tribo-materials and water had occurred. Here the thin water lubrication film easily broke down and solid-to-solid contact was established. Then there was boundary lubrication in friction area. This led the friction coefficient to increase. Thus, the wear mechanism in the second area (II) was mechanical wear with partial tribochemical wear (MW+PTW). If the experimental parameters were located in the third area (III), the friction coefficient varied in the range of 0.004~0.029 and the specific wear rate of the a–CN_x coatings and Si_3N_4 balls fluctuated in the range of 3.2×10^{-8}~9.0×10^{-8} and 1.4×10^{-8}~3.5×10^{-8} mm^3/Nm. The worn surfaces of Si_3N_4 ball and the a–CN_x coating had become smooth and were covered with shallow scratches (Fig. 14). This indicated that a tribochemical reaction had occurred. Thus, the wear mechanism in here was tribochemical wear with slight partial mechanical wear (TW+PMW). If the sliding wear tests were performed at the highest sliding velocity (Area IV), friction coefficients less than 0.01 and specific wear rates lower than 6.6×10^{-8} mm^3/Nm for the a–CN_x coatings and 3.0×10^{-8} mm^3/Nm for Si_3N_4 balls were

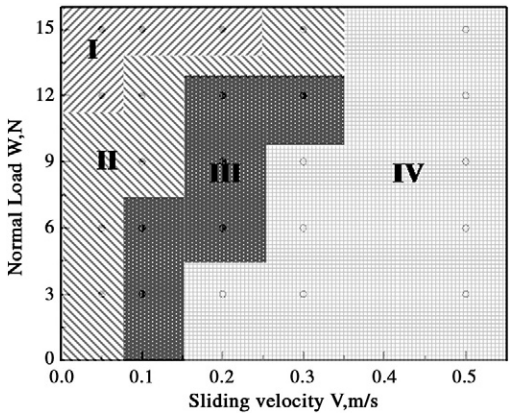

Fig. 11. Wear-mechanism map of the a–CN_x coatings sliding against Si_3N_4 balls in water.

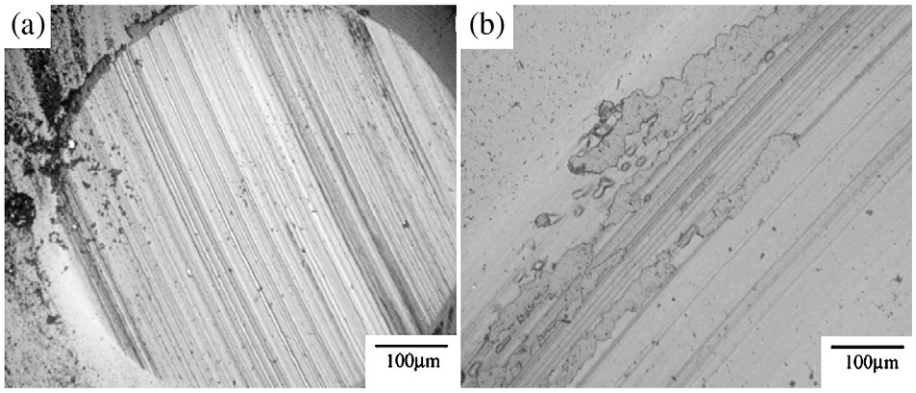

Fig. 12. Wear scar on Si_3N_4 ball (a) and wear track surface on the a–CN_x coating (b) after sliding in water at 15 N and 0.05 m/s.

obtained, and smooth and flat worn surfaces were observed (Fig. 15). This made clear that the tribochemical reaction occurred easily, and the $SiO_2{\cdot}xH_2O$ gels acted as lubrication film, which was beneficial to providing super lubricity to the self-mated Si_3N_4 tribopairs in water [4,8,10]. Thus, the lubrication mechanism was hydrodynamic lubrication and the wear mechanism was tribochemical wear (TW) in the fourth zone.

3.7. Discussion

For the a–CN_x/Si_3N_4 tribo-couple, the hardness of the a–CN_x coatings is 29 GPa, higher than that of Si_3N_4 balls (15.3 GPa). According to normal friction and wear theory, the specific wear rate of the Si_3N_4 balls should be higher than that of the a–CN_x coatings. But in here, the specific wear rates of Si_3N_4 ball were lower than those of the a–CN_x coatings. This was related to transfer of a tribo-layer from coating to the ball [26]. However, in comparison with Ref.[15,21], it is easily found that a lower friction coefficient was obtained for SiC/SiC, Si_3N_4/Si_3N_4 and a–CN_x/SiC(Si_3N_4) tribo-couples, but the specific wear rates of tribo-materials in the a–CN_x/SiC(Si_3N_4) tribo-couples were all lower than those of tribo-materials in the SiC/SiC and Si_3N_4/Si_3N_4 tribo-couples. For the a–CN_x/SiC(Si_3N_4) tribo-couples in water, the wear rate of SiC ceramic ball was lower than that of Si_3N_4 ceramic ball [18]. This indicated that the hydration reaction of Si_3N_4 in water occurred easily. Thermodynamic calculations of the phase equilibrium within the interface showed that water did not react with SiC or Si_3N_4 in the presence of oxygen. Since the water was saturated with oxygen and oxygen was therefore present in the tribocontact, the following Eqs. (3) and (4) most likely took place. ΔG_f^{298} is the Gibbs free energy of formation at 298 K.

$$SiC+2O_2 \rightarrow SiO_2+CO_2 \quad \Delta G_f^{298} = -589\text{kJ/mol} \tag{3}$$

$$Si_3N_4+3O_2 \rightarrow 3SiO_2+2N_2 \quad \Delta G_f^{298} = -1779.4\text{kJ/mol}. \tag{4}$$

From Eqs. (3) and (4), it is clear that the formation of SiO_2 film which evolved from Si_3N_4 was expected to be more rapid than SiC tribopairs. The oxides could be hydrated by association with an undetermined amount of water molecules to form $SiO_2 \cdot xH_2O$ gels. Such films have been described specifically in the wear experiments of SiC/SiC and Si_3N_4/Si_3N_4 tribo-couples running in moist air [4]. For SiO_2, a subsequent dissolution reaction in the tribo-contact would also be expected to occur:

$$SiO_2+2H_2O \rightarrow Si(OH)_4 \quad \Delta G_f^{298} = -237\text{kJ/mol}. \tag{5}$$

If the hydration reaction between Si_3N_4 or SiC ceramic and water occurred directly, we could calculate from Eqs.(6) and (7)

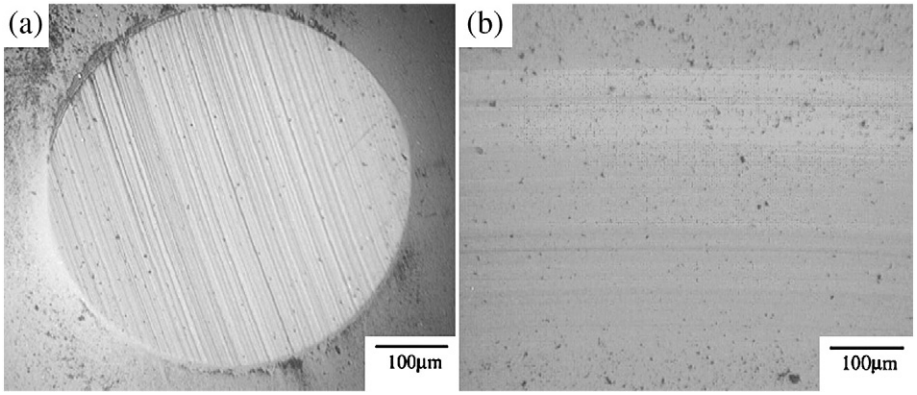

Fig. 13. Wear scar on Si_3N_4 ball (a) and wear track surface on the a–CN_x coating (b) after sliding in water at 12 N and 0.1 m/s.

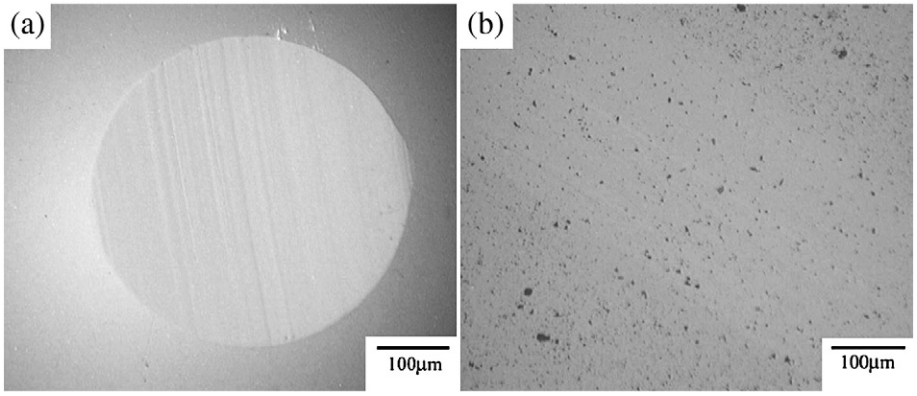

Fig. 14. Wear scar on Si_3N_4 ball (a) and wear track surface on the a–CN_x coating (b) after sliding in water at 6 N and 0.1 m/s.

that silicon nitride was more easily hydrated than silicon carbide.

$$SiC+4H_2O\rightarrow Si(OH)_4+CH_4 \quad \Delta G_f^{298}=-598.91kJ/mol \qquad (6)$$

$$Si_3N_4+12H_2O\rightarrow 3Si(OH)_4+4NH_3 \qquad (7)$$
$$\Delta G_f^{298}=-1268.72kJ/mol$$

This might be attributed to more wear loss on Si_3N_4 than SiC. Refs. [8, 27] proposed that, when a very low friction coefficient was obtained for self-mated Si_3N_4 tribopairs, there mainly existed $Si(OH)_4$ gels and water film between pin and disk, while for self-mated SiC tribopairs, there existed a SiO_2 film and water film between the two contacting surfaces. Thus, we could conclude that, after the water lubrication film broke down and the $Si(OH)_4$ gels were removed, solid-to-solid contact for the a–CN_x/Si_3N_4 tribopair was established. Thus, the friction coefficient increased abruptly and the lubrication mechanism changed from ML into BL. However, for the a–CN_x/SiC tribo-couples, the SiO_2 film acted as a 'lubricant' on the worn surface to prevent direct contact of bulk materials, so HL changed into ML and then gradually changed into BL [19].

Otherwise, the a–CN_x coatings offered higher values of H/E and a combination of reasonably high hardness and suitable stiffness. Hence they possessed excellent tribological properties [20]. If the Si_3N_4 disk was covered with amorphous carbon nitride coatings, friction would transform the surface layer of the a–CN_x coating and give it lower shear strength, which is responsible for low friction and the transfer of material. When Tanaka A. et al. [28,29] studied the friction and wear property of DLC coatings in water, they indicated that the structure of transferred materials was very different from that of the original DLC film and similar to that of polymer-like carbon, which is softer in comparison to DLC film. The amount of transferred material with the polymer-like structure was larger in water than in air. But for a–CN_x coatings, the surface structure of the a–CN_x films was found to become C sp^2-bond-rich structures [18,20, 30–32]. Hellgren et al. [33] have reported that if operated in the presence of oxygen or hydrogen, those elements would react with a–CN_x film and promote decomposition. This indicates that the decomposition of the a–CN_x coatings occurred during sliding in water. After nitrogen atoms were removed from the a–CN_x coatings, the sp^2-bonding-rich structure surface with lower shear strength was formed on the worn surface of the a–CN_x films and carbon bonds could be terminated with OH^- in water, which was also responsible for low friction for the a–CN_x/SiC(Si_3N_4)tribo-couple, and low wear rate of the SiC(Si_3N_4) ball in water.

4. Conclusions

The influences of normal load and sliding speed on the friction and wear property of a–CN_x coatings sliding against

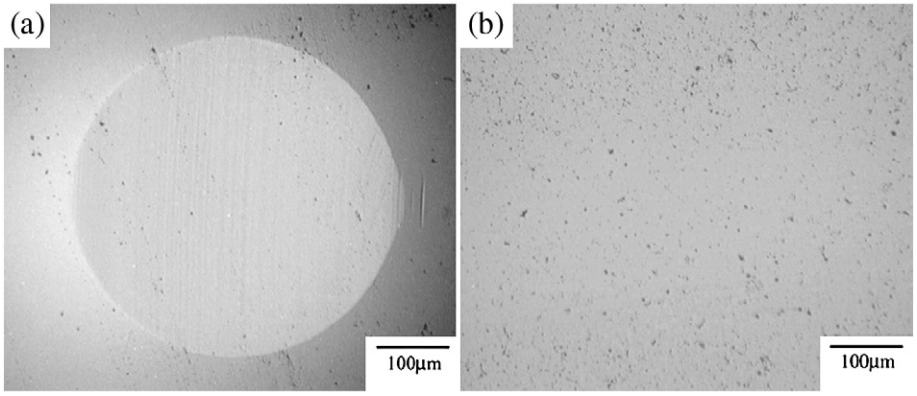

Fig. 15. Wear scar on Si_3N_4 ball (a) and wear track surface on the a–CN_x coating (b) after sliding in water at 9 N and 0.5 m/s.

Si_3N_4 balls in water have already been investigated in detail. The main results could be summarized as:

1. The a–CN_x coatings contained 12 at.% nitrogen and their structure was a mixture of $sp^2$and sp^3 bonds. The nano-hardness of the a–CN_x coatings was 29 GPa.
2. The influences of the sliding speeds on the friction coefficients and the specific wear rate of the CN_x coatings were more obvious than those of the normal loads. The friction coefficients and the specific wear rate of the CN_x coatings decreased as the sliding speed increased, while the normal load and sliding speed had no obvious influence on the Si_3N_4 ball's specific wear rate.
3. At the sliding velocity higher than 0.1 m/s, the friction coefficient of the a–CN_x/Si_3N_4 tribo-pair in water was smaller than 0.04. The mean steady-state friction coefficient fluctuated slightly in the range of 0.001~0.006 at 0.5 m/s.
4. When the sliding speed was lower than 0.1 m/s, the specific wear rates of the a–CN_x coatings were higher than those of Si_3N_4 balls. If the sliding speed was higher than 0.2 m/s, the specific wear rates of the a–CN_x coatings and the Si3N4 balls all fluctuated around a lower level of 10^{-8} mm3/Nm.
5. The wear-mechanism map for the a–CN_x/Si_3N_4 tribo-pair in water was developed at the normal loads of 3~15 N and the sliding speeds of 0.05~0.5 m/s: (I) Mechanical wear; (II) Mechanical wear+Partial tribochemical wear; (III) Tribochemical wear+Partial mechanical wear; (IV) Tribochemical wear.

Acknowledgements

This work was supported by Japan Society for the Promotion of Science under Grant-in-Aid for Scientific Research (JSPS Fellows P03219) and National Natural Science Foundation of China (NNSFC) (No.50675102) as well as Natural Science Foundation of Jiangsu Province (No.BK2007529). We would like to acknowledge JSPS and NNSFC as well as NSFJP for financial support.

References

[1] M. Masuko, A. Suzuki, Y. Sagae, M. Tokoro, K. Yamamoto, Tribol. Int. 39 (2006) 1601.
[2] A. Iwabuchi, International Tribology Conference, Kobe, June, 2005.
[3] C. Long, X. Wang, J. Mater. Sci. 39 (2004) 1499.
[4] H. Tomizawa, T.E. Fischer, ASLE Trans. 30 (1987) 41.
[5] F. Honda, T. Saito, Appl. Surf. Sci. 92 (1996) 651.
[6] J.F. Li, J.Q. Huang, S.H. Tan, Z.M. Cheng, C.X. Ding, Wear 218 (1998) 167.
[7] H. Wong, N. Umehara, K. Kato, Wear 218 (1998) 237.
[8] J. Xu, K. Kato, Wear 245 (2000) 61.
[9] R. Wäsche, D. Klaffke, Tribol. Int. 32 (1999) 197.
[10] M. Chen, K. Kato, K. Adachi, Tribol. Int. 35 (2002) 129.
[11] R.D. Amutha, Y. Yoshizawa, H. Hyuga, K. Hirao, Y. Yamauchi, J. Eur. Ceram. Soc. 24 (2004) 3279.
[12] H. Hyuga, M. Jones, K. Hirao, Y. Yamauchi, J. Am. Ceram. Soc. 88 (2004) 699.
[13] H. Hyuga, K. Hirao, H. Kita, M. Jones, Y. Yamauchi, J. Am. Ceram. Soc. 88 (2005) 3474.
[14] T. Saito, T. Hosoe, F. Honda, Wear 247 (2001) 233.
[15] F. Zhou, K. Kato, K. Adachi, Tribol. Lett. 18 (2005) 153.
[16] D.A. Ersoy, M.J. McNallan, Y. Gogotsi, A. Erdemir, Tribol. Trans. 43 (2000) 809.
[17] B. Carroll, Y. Gogotsi, A. Kovalchenko, A. Erdemir, M.J. McNallan, Tribol. Lett. 15 (2003) 51.
[18] F. Zhou, K. Adachi, K. Kato, Diamond Relat. Mater. 14 (2005) 1711.
[19] F. Zhou, K. Adachi, K. Kato, Surf. Coat. Technol. 200 (2006) 4909.
[20] F. Zhou, K. Adachi, K. Kato, Thin Solid Films 514 (2006) 231.
[21] F. Zhou, X. Wang, K. Kato, Z. Dai, Wear 263 (2007) 1253.
[22] S. Toyokawa, Master Thesis, Tohoku Univ. (2003) 92.
[23] D. Beeman, J. Silverman, R. Lynds, M.R. Anderson, Phy. Rev. B30 (1984) 870.
[24] S. Zhang, X.L. Bui, Y. Fu, D.L. Butler, H. Du, Diamond Relat. Mater. 13 (2004) 867.
[25] W.C. Oliver, G.M. Pharr, J. Mater. Res. 7 (1992) 1564.
[26] K. Jia, Y.Q. Li, T.E. Fischer, B. Gallois, J. Mater. Res. 10 (1995) 1403.
[27] M. Chen, K. Kato, K. Adachi, Tribol. Int. 35 (2002) 129.
[28] M. Suzuki, T. Ohana, A. Tanaka, Diamond Relat. Mater. 13 (2004) 2216.
[29] A. Tanaka, M. Suzuki, T. Ohana, Tribol.Lett. 17 (2004) 917.
[30] J. Wei, P. Hing, Z.Q. Mo, Wear 225–229 (1999) 1141.
[31] J.C. Sanchez-Lopez, C. Donnet, T. Le Mogne, Vacuum 64 (2002) 191.
[32] J.C. Sanchez-Lopez, M. Belin, C. Donnet, C. Quiros, E. Elizalade, Surf. Coat. Technol. 160 (2002) 138.
[33] N. Hellgren, N. Lin, E. Broitman, V. Serin, S. Grillo, R. Twesten, I. Petrov, C. Colliex, L. Hultman, J. Sundgren, J. Mater. Res. 16 (11) (2001) 3188.